Trans. JWRI, Vol. 23 (1994), No. 2

Effect of M-A Constituent on Fracture Behavior of 780 and 980 MPa Class HSLA Steels Subjected to Weld HAZ Thermal Cycles†

Fukuhisa MATSUDA*, Kenji IKEUCHI, Hitoshi OKADA *****
Ivan HRIVNAK** and Hwa-Soon PARK*******

Abstract

In order to explain the embrittlement of 780 and 980 MPa class HSLA steels undergoing high heat input weld thermal cycle, the effects of the M-A constituent on the initiation and propagation of fracture have been investigated metallographically and theoretically. The M-A constituent was observed both at initiation sites of cracks in the cleavage fracture and at the bottom of dimples in the ductile fracture. This suggests that the M-A constituent acts as an initiation site for both cleavage fracture and dimple fracture. FEM analyses of strain in the α phase involving M-A constituents show that under a tensile load the concentration of tensile-plastic strain occurs over a wider area around massive M-A constituents than around elongated ones having the same length. This can explain the result from the instrumented-Charpy impact test that the massive M-A constituent reduced the fracture-initiation energy more significantly than the elongated. The instrumented-Charpy impact test also suggested that the fracture-initiation and propagation energies were lowered more significantly with an increase in the massive M-A constituent. Since cracks in the Charpy impact test were observed to propagate preferentially along the M-A constituent/matrix interface, it can be considered that the increase in the area of the interface is responsible for the decrease in the initiation and propagation energy of fracture because of the increase in the amount of the massive M-A constituent.

KEY WORDS: (High Strength Steel) (Weld Simulation) (M-A Constituent) (Toughness)

1. Introduction

According to previous reports[1-3] on the initiation condition of voids at the initial stage of ductile fracture, it has been suggested that the initiation of voids is generally caused by the internal stress due to the difference in plastic strains which occurs between the second phase and the matrix. It has also been suggested[1,2] that the degree of internal stress generated depends not only on the volume fraction, shape and size, absorbed energy of the second phase[1,2] but also on its yield strength or plastic deformation capability[3]. Furthermore, according to reports[4-6] concerning the relation between the carbide and initiation behavior of cleavage fracture, micro-fractures are initiated mainly by cracking of the carbide itself. The initiated micro-crack may become larger and propagate to cause cleavage fracture, and the size of plastic zone at the tip of the micro-crack may play an important role in the initiation behavior of cleavage fracture. Moreover, it has been said that the larger carbide is more prone to act as an initiation site of cleavage fracture[4-7].

In previous papers[8-10], the authors have reported that the M-A(Martensite-Austenite) constituent can be classified into elongated and massive types according to their shape[8], and suggested that the massive M-A constituent impairs the toughness of weld HAZ more seriously[8-10]. With respect to the effect of the M-A constituent on the toughness, Yoneda[11] and Nakanishi et al[13] have suggested that the M-A constituent acts as an initiation site for a crack and also promotes its propagation.

In order to explain the impairment of the toughness by the M-A constituent, we have carried out a FEM analysis of plastic strain around M-A constituent by assuming that it is an elongated or massive particle,

† Received on November 25, 1994
* Professor
** Associate Professor
*** KURIMOTO Ltd., Osaka
**** Visiting Professor(Technical Univ. in Kosice, Kosice, Slovakia)
***** Pusan National Univ. of Tech., Pusan, Korea
Transactions of JWRI is published by Welding Research Institute, Osaka University, Ibaraki, Osaka 567, Japan

much harder than the matrix.

It has already been reported that the hardness of M-A constituents is very high compared with the matrix[9], and it is generally said that a harder phase has higher tensile strength[15]. Therefore, it can be presumed that the yield strength also increases with the hardness. If tensile stress is applied to a steel containing M-A constituent, an excessive internal stress will be generated in the matrix nearby the constituent because of the concentration of plastic strains resulting from the difference in their yield strengths, (as long as the M-A constituent itself is not cracked).

In this report, the effects of the M-A constituent on initiation and propagation of fracture have been investigated by the observation of crack behavior and by the FEM analysis of strain distribution around the M-A constituent.

2. Experimental Details

2.1 Test material

The chemical compositions of the steel plates used are shown in Table 1. Steels HT80-A and HT80-B are 780 MPa class high tensile steels and HT100-B is a 980 MPa class.

2.2 Test methods

In order to investigate the effect of cooling rate on the dimensions of M-A constituent, not less than 30 massive and elongated M-A constituents were observed by the TEM replica method. The dimensions of M-A constituent are expressed as the average values of width W and length L. The average area of M-A constituent(A_{eq}) is defined as W_{av} X L_{av}(W_{av} and L_{av} are average values of W and L, respectively).

A slow rate bending test and Charpy impact test with a small applied energy were used to investigate the effect of M-A constituent on the ductile fracture and the cleavage fracture. The shape of test pieces used for the test was of 10 X 10mm square section with the length of 55mm, and a single weld thermal cycle with cooling time from 1073 to 773 K $\Delta t_{8/5}$=200s[8] was applied to them.

In the slow rate bending test, the bending loads were applied to the test piece with a bending radius of 10mm on its compression side and a maximum strain rate of 0.3mm/s. The impact test was carried out using applied impact energies of 40J or less, so that the test specimen would not be completely broken. Prior to the tests, the specimens were metallographically polished, and the M-A constituent was revealed by etching with 2% Nital. Some specimens were tested without etching, so that the M-A constituent on both the fractured surface and the polished surface could be observed by etching with 2% Nital after the tests.

The chemical composition of the M-A constituent was analyzed with EPMA and the ZAF method (atomic number correction, absorption correction and fluorescence correction). Because of the effective beam diameter of EPMA (2–3μm), M-A constituents larger than the beam diameter were chosen carefully for the analysis.

The initiation and propagation energies of fracture were estimated from a load-displacement curve of an instrumented- Charpy test. The capacity of the test machine was 480J. The test pieces were 2mm V-notched test pieces which had been given the simulated weld thermal cycle. From the average of values for three test specimens, the fracture initiation and propagation energies were estimated in vE. The test temperature was 283 K[8].

3. Numerical Analysis

The numerical analysis of the strain near the M-A constituent under a tensile load was carried out by the elastic-plastic finite element method. The model for the analysis is shown in Fig. 1 and Table 2. The minimum mesh dimensions used were (A/200) X (B/125).

Region I in Fig. 1 represents the soft phase, viz., the (α) ferrite matrix, and region II represents the hard phase, viz., the M-A constituent. The analysis has been carried out under plane stress conditions with the assumption that the hard second phase exists in the soft matrix and the both phases are isotropic and homogeneous. For the symmetry, the analysis has been carried out for a 1/4 model. The value and distribution of

Table 1 Chemical compositions of steel plates used.

Material	Thickness	Chemical compositions (mass%)													Ceq	Pcm
	mm	C	Si	Mn	P	S	Cu	Ni	Cr	Mo	V	Nb	Al	B		
HT80-A	60	0.12	0.23	0.93	0.006	0.002	0.19	1.22	0.48	0.45	0.03	-	0.066	0.0007	0.53	0.26
HT80-B	25	0.10	0.27	0.92	0.009	0.002	0.20	0.98	0.47	0.27	0.04	-	0.052	0.0012	0.45	0.23
HT100-B	38	0.11	0.11	0.86	0.004	0.001	0.03	1.57	0.54	0.56	0.073	-	0.053	0.0011	0.55	0.26

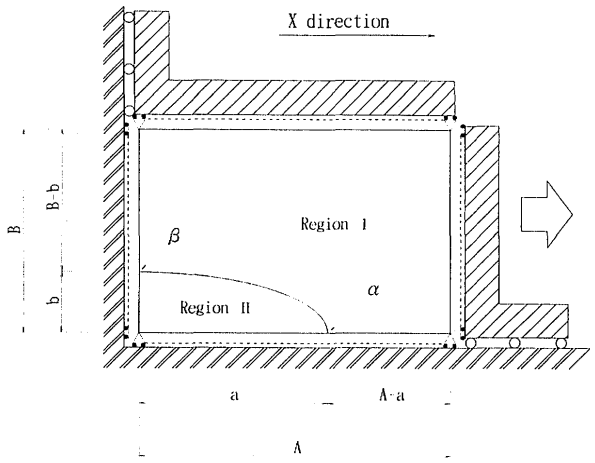

Fig. 1 Shape of analyzed model.

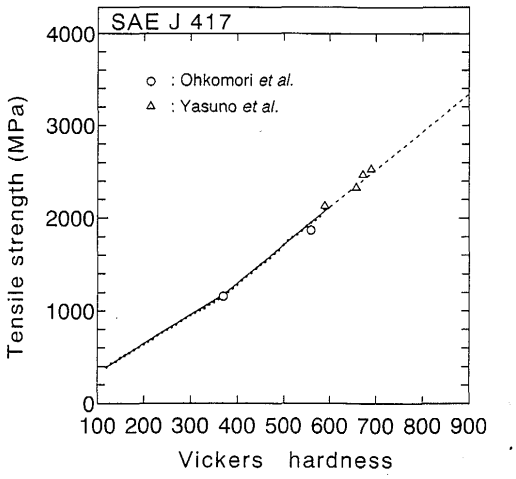

Fig. 2 Relation between Vickers hardness and tensile strength of SAE J417.

Table 2 Dimensions of analyzed model in Fig. 1.

Case No.	A	a	A-a	B	b	B-b	Aspect ratio of region II	Area fraction of region II	Element number	Node number
1	10	5	5	5	3.33	1.67	1.5	26.2	851	2658
2	10	5	5	5	0.5	4.5	10	3.93	591	1865

Table 3 Mechanical properties of analyzed model.

Region	Aspect ratio	Element	Young's modulus 10^4N/mm^2	Strain-hardening exponent 10^3N/mm^2	Poisson ratio	Yield strength MPa
Region II	<3	Massive M-A	20.10	0.98	0.28	3200
	≧3	Elongated M-A	20.30	0.98	0.28	2400
Region I	——	Ferrite	20.80	0.98	0.29	450

tensile plastic strain were calculated under a load producing forced displacements 5% or less in the X direction. The values of the parameters used for the analysis are shown in Table 3.

From preliminary experiments the aspect ratios(L_{av}/W_{av}) of elongated M-A and massive M-A constituents were estimated to be 10 and 1.5, respectively.

Young's modulus and Poisson's ratio of the hard phase were estimated as follows. According to the observation[9] with TEM, the amount of residual γ-phase in the massive and elongated M-A constituents is much smaller than the amount of martensite. Therefore, the analysis has been carried out assuming that the M-A constituent consists only of the martensite.

Speich et al.[16] have studied the effect of alloying elements of Ni, Cr, Mn, and C on the elastic modulus, rigidity and Poisson's ratio of the martensite. They showed that the content of carbon (<2.3 mass %) had a very strong influence on the Young's modulus, while the effects of the other alloying elements were negligible. They also showed that Poisson's ratio was hardly affected by the addition of alloying elements. Young's modulus and Poisson's ratio of the massive and elongated M-A constituents were estimated from the C content of the M-A constituent determined in a previous paper[9] and incorporating Speich et al's results.

The yield strength of the M-A constituent was estimated as follows. Conversion table of hardness, SAE J 417, gives the approximate value of tensile strength corresponding to the hardness up to Hv=595. The relation between the tensile strength and hardness is shown as a solid line in Fig.2. The broken line in Fig.2 shows the extrapolation of the relation given by SAE J 417 up to Hv=900. Experimental data from maraging steel[17] and high strength roll steel[18] for Hv=370-700 are also shown in Fig. 2, and are in good agreement with the relation given by SAE J 417.

The hardness (Hv) of massive and elongated M-A has been determined to be 900 and 700 respectively in a previous paper[9]. From Fig. 2, the tensile strengths corresponding to Hv=900 and 700 are 2,520 MPa and 3,350 MPa respectively. The yield strength of M-A constituent was then assumed to be 95% of the tensile strength (see Table 3). The yield point has been judged by using Mises's yielding conditions assuming that the coefficient of work hardening is 980 N/mm^2 [19,20].

4. Experimental Results and Discussion

4.1 Effect of cooling rate on shape of M-A constituent

The length (L_{av}), width (W_{av}) and area (A_{eq}) of the M-A constituent formed in the simulated CGHAZ of HT80-A, HT80-B and HT100-B are shown as a function of cooling time $\Delta t_{8/5}$ in Figs.3(a)-3(c).

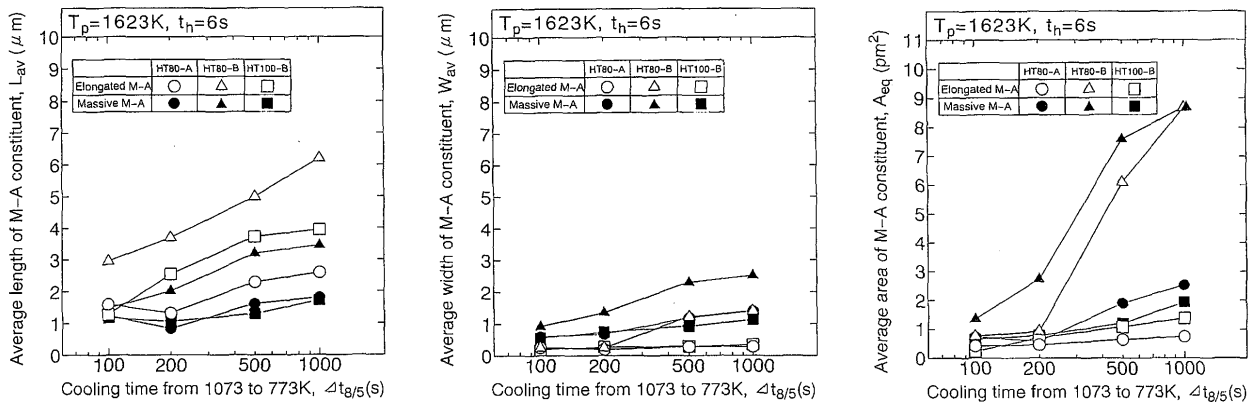

Fig. 3 Relation between $\Delta t_{8/5}$ and shape of M-A constituent.

As shown in Fig. 3(a), with the increase in $\Delta t_{8/5}$, length L_{av} tended to increase for both massive and elongated M-A constituents in all the steels used. Length L_{av} of the elongated M-A was larger than that of the massive M-A, and L_{av} in HT80-B was much larger than those of the other steels. Width W_{av} of the elongated M-A in HT80-A and HT100-B steels was almost independent of $\Delta t_{8/5}$ as shown in Fig. 3(b). In contrast, W_{av} in the HT80-B steel increased with the increase in $\Delta t_{8/5}$, and W_{av} of the massive M-A in HT80-B was much larger than the other two steels. Area A_{eq} of the M-A constituent in HT80-A and HT100-B steels slightly increased with $\Delta t_{8/5}$ as shown in Fig. 3(c). In HT80-B steel, A_{eq} of both the elongated and massive M-A constituents increased dramatically with $\Delta t_{8/5}$ when $\Delta t_{8/5}$ exceeded 200s.

Since the M-A constituent is formed from the austenite in the final stage of transformation during the cooling process, it may be thought that the formation of the M-A constituent is closely related to the growth of α phase during the cooling process, namely the hardenability of steel. According to observations with the optical microscope, no boundary α phase was formed even for $\Delta t_{8/5}$ of 500s in the HT80-A or HT100-B steels, and the M-A constituent was formed between lath-shaped α phases. However, in HT80-B steel, a boundary α phase was formed, but the lath-shaped α phase could not be clearly observed even for $\Delta t_{8/5}$ of 200s or more. In this steel, lots of coarse massive M-A constituent were formed. Since the hardenability of HT80-B steel was lower than those of HT80-A and HT100-B steels, the boundary α phase and the intergranular elongated α phase grew easily in HT80-B steel. It is conceivable that intergranular elongated α phases grow to contact with each other, leaving untransformed γ phase regions of an elongated shape among them. The massive M-A constituent was probably formed from the untransformed γ region of a massive shape during the cooling process. This may explain why the M-A constituent formed in the HT80-B steel was larger than those in the HT80-A and HT100-B. It can therefore be concluded that the difference in the shape of the M-A constituent among the steels employed is caused by the differences in their hardenability.

The changes in the shape and the total area of M-A constituent with cooling time $\Delta t_{8/5}$ show that the increase reported in a previous paper[8] is attributable to the growth of the M-A constituent rather than an increase in their numbers. Therefore, the growth of the massive M-A constituent may explain the observed influence of the amount of the M-A constituent on the fracture behavior.

4.2 Effect of M-A constituent on ductile fracture

M-A constituents near fracture surfaces of the HT80-B steel subjected to a slow rate bending test at 283 K were observed with the SEM. As shown in Figs. 4(a) and 4(b), the elongated M-A constituents indicated with arrows underwent heavy plastic deformation, suggesting that in some cases the elongated M-A constituent can deform plastically and absorb strain energy without cracking even if a large bending strain is given.

On the other hand, lots of M-A constituents were also observed which were cracked and fragmented with only slight deformation. The example of the elongated M-A constituents which were cracked and fragmented with slight deformation is shown in Fig. 5(arrow mark). Chen et al.[11] have reported similar cracked and fragmented M-A constituents in a specimen that received a simple tension force.

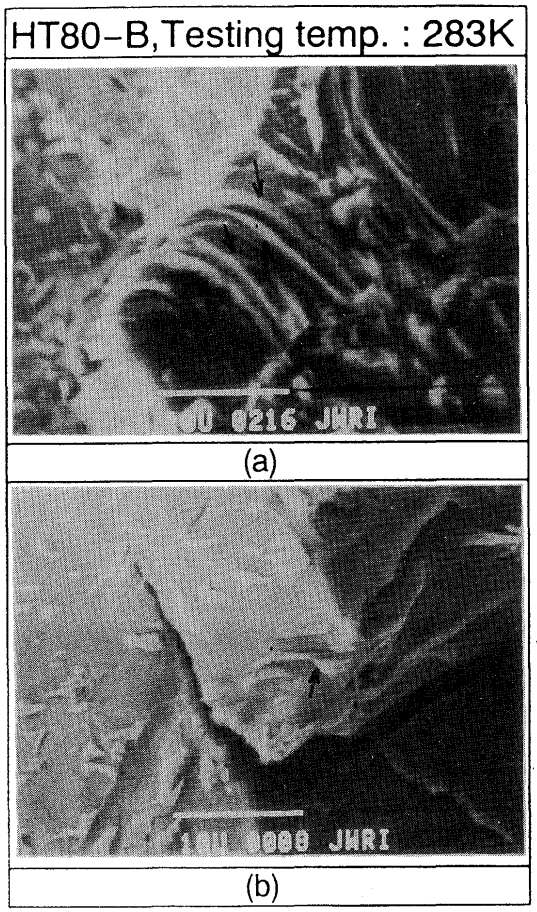

Fig. 4 Morphology of heavily strained M-A constituent near the fracture surface of HT80-B.

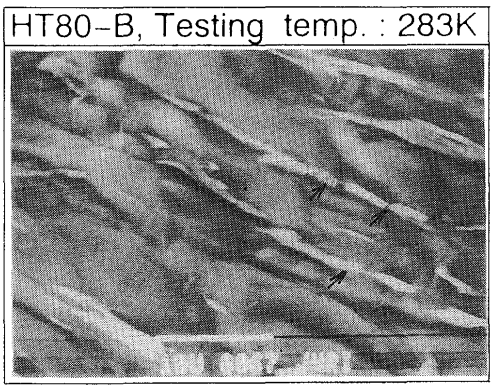

Fig. 5 Morphology of heavily strained M-A constituent near the fracture surface of HT80-B.

From the observation of many M-A constituents in specimens subjected to the slow rate bending test, it can be concluded that more elongated M-A constituents were cracked than massive M-A constituents. This is consistent with Tomota et al's[3] observation that the coarse-second-phase crack occurs more frequently in a narrow martensite colony which is longitudinally extended in the tensile direction.

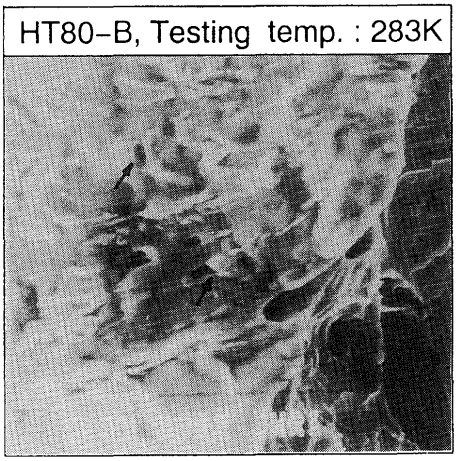

Fig. 6 Microvoid initiation in HT80-B after bending test.

In addition to the crack, micro voids were also observed as shown in Fig. 6. The initiation of micro voids in the neighborhood of the interface between elongated M-A constituent and matrix are indicated with arrows in Fig. 6. Where the degree of the deformation is increased, these micro voids are probably connected with each other, and form cracks resulting in plastic fracture.

It is said that the size of dimples on the ductile fracture surface depends on both the number of micro void initiation sites available and the relative plasticity of the matrix. In order to consider the role of the M-A constituent in the ductile fracture, the distribution of the M-A constituent on a fractured surface of a slow rate bending test specimen was revealed by Nital etching.

Particles which could be regarded as the M-A constituent could be observed inside the dimple as shown in Fig. 7.

In fact, the carbon content of the particle at the bottom of the dimple was estimated to be 1.10 - 1.64 mass % following EPMA analyses. The measured value of the carbon content lies within the range of the carbon

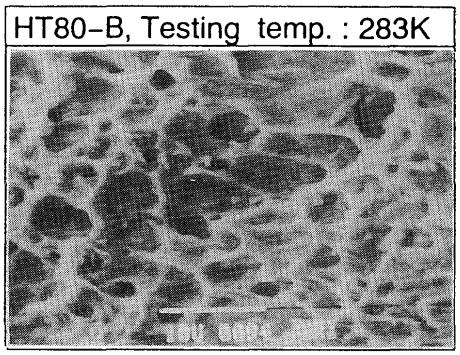

Fig. 7 Microstructure of dimple fractured surface revealed by etching with nital solution. Notice that M-A constituent is observed in each dimple.

content of the M-A constituent[9]. These results suggest that the M-A constituent exists at the bottom of the dimple.

4.3 Effect of M-A constituent on cleavage fracture

It has been pointed out by several authors[13,21] that the M-A constituent exists at the initiation site of main and secondary cracks of the cleavage fracture. EPMA analyses were made to estimate the carbon content at places which appeared to be the initiation sites of cleavage fracture. The analyzed area and the result from the analysis are shown in Fig. 8. A particle with a carbon content as high as 1.44 mass % has been detected, suggesting that a M-A constituent is present at the initiation site of cleavage cracks[9].

It has also been said that the M-A constituent aids the propagation of cleavage fractures[11-14,21]. As shown in Fig. 9, M-A constituents on the cleavage fractured surface(right-hand field) and its cross section(left-hand field) were revealed by Nital etching. Though many M-A constituent were observed on the fracture surface as shown in Fig. 9, only small amount of M-A constituents were cracked and fragmented. This result suggests that the cleavage fracture propagates preferentially along the interface between the M-A constituent and matrix in accord with the previous reports[11-14,21].

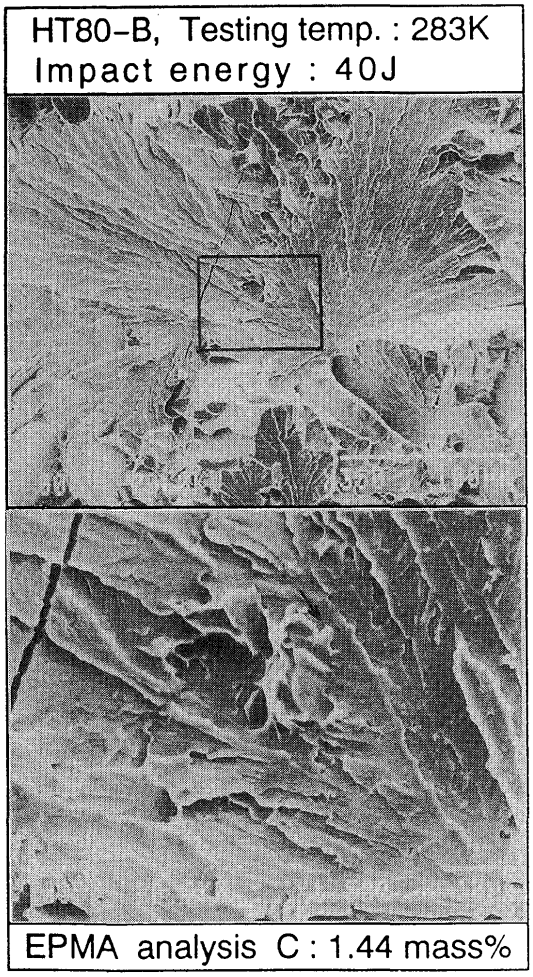

Fig. 8 C-content analyzed with EPMA at the initiation site of cleavage fracture of HT80-B.

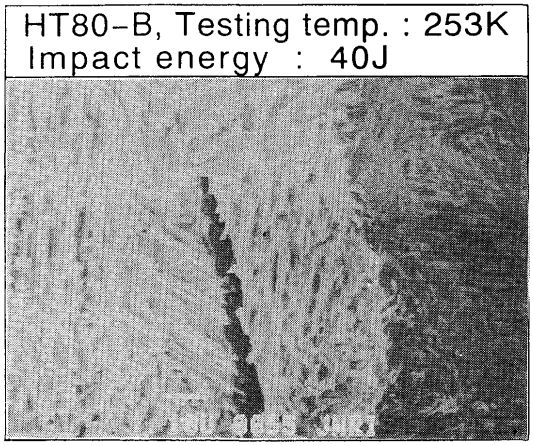

Fig. 9 Microstructure of cleavage fracture surface revealed by etching with nital solution.

4.4 Effect of M-A constituent on crack initiation and propagation energies

Crack initiation and propagation energies of the base metal of HT80-B steel and its simulated CGHAZ were estimated with the instrumented-Charpy impact test. Cooling times $\Delta t_{8/5}$ of the simulated thermal cycle of CGHAZ are 50 and 200s. As shown in Table 4, the crack propagation energy was about twice as large as the crack initiation energy for the base metal.

When $\Delta t_{8/5}$ was 50s, i.e., when only elongated M-A constituent was formed[8], the crack initiation energy of the simulated CGHAZ was comparable to that of the base metal. This result suggests that the elongated M-A constituent has only slight influence on the crack initiation energy. Although the crack propagation energy of the CGHAZ of $\Delta t_{8/5}$=50s was decreased considerably, the total absorbed energy still satisfied the required toughness ($vE_0 \geq 47J$) of the 780MPa class high tensile steel for penstocks[22] and bridges[23]. The microstructure of the base metal consisted mainly of the tempered

Table 4 Result of instrumented-Charpy testing in HT80-B.

$\Delta t_{8/5}$ s	Total vE J	vE for crack initiation (J)	vE for crack propagation (J)	Area fraction of M-A constituent (%)
50	260	111	130	E:11 , M: 0
200	31	20	7	E: 7 , M:17
(Base metal)	375	105	218	E: 0 , M: 0

E: Elongated M-A constituent
M: Massive M-A constituent

martensite and B-III type bainite which were of excellent toughness[24], but when $\Delta t_{8/5}$=50s, the microstructure of the matrix of the CGHAZ consisted of the B-III type bainite and B (I,II) type bainite which was inferior in toughness. The difference in these microstructures should also be taken into account to explain the lower crack propagation energy of the simulated CGHAZ when $\Delta t_{8/5}$=50s. These results suggest that although the elongated M-A constituent lowers the crack propagation energy, its influence is not significant from the practical point of view.

On the other hand, when $\Delta t_{8/5}$ was 200s, the fraction of massive M-A constituent became larger than that of elongated M-A constituent, and both crack initiation energy and propagation energy were decreased significantly as compared with those of $\Delta t_{8/5}$=50s. When $\Delta t_{8/5}$=200s, the microstructure of the matrix consisted mostly of B-I type bainite. Though the B-I type bainite has been said to cause a significant decrease in the toughness[28], we think the massive M-A constituent decreases the crack initiation and propagation energies much more significantly than the elongated M-A constituent.

5. Results of Numerical Calculation and Discussion

The effect of the shape of the hard phase on the distribution of tensile-plastic strain in the surrounding soft phase is shown in Fig. 10. In this figure, the contour map of the maximum principal tensile-plastic strain is represented in different colors. The applied strain for this result is 5% in the X direction. The arrows in the figure indicate the interface between the hard and soft phases.

As can be seen in Fig. 10, the plastic strain concentrates significantly in the soft phase next to the hard phase for both elongated shape and massive shape. These results correspond well with the experimental observations that micro-voids were initiated in the neighborhood of the interface between M-A and matrix as shown in Fig. 6. The region of the large tensile plastic strain extends over wider area around massive hard phases than around elongated hard phases.

There have been many papers reporting of the effect of the M-A constituent on toughness. Several authors have said that the size of M-A constituent is a controlling factor in fracture initiation[11,12,26,27], and the increase in the size of the M-A constituent lowers the critical fracture stress[11,12]. It has also been suggested that the amount of the M-A constituent is a more important factor for the fracture initiation. According to the results described above, the M-A constituent increased as $\Delta t_{8/5}$ was increased, and this tendency was more significant for the massive M-A constituent than for the elongated M-A.

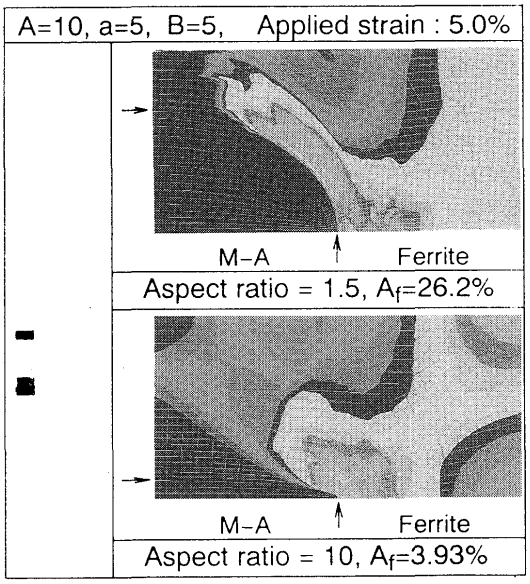

Fig. 10 Morphology of plastic strain concentration at the tip of M-A constituent.

Furthermore, provided that the longest axes are of the same length, the area of high tensile plastic-strain region set up in the soft phase is wider for the massive hard phase than for the elongated (see Fig. 10). Therefore, large micro-voids and/or micro-cracks can initiate more easily in the α phase matrix near the massive M-A constituent compared with the elongated. This implies that the probability of the occurrence of cracks satisfying Griffith's conditions is higher around the massive M-A constituent than the elongated. The increase in the dimensions of micro-cracks occurring around the massive M-A constituent can probably explain why fracture can be initiated with a smaller energy around the massive M-A constituent.

With respect to the effect of the M-A constituent on the crack propagation, Yoneda[13] has emphasized the stress concentration at the interface between M-A constituent and matrix, and Nakanishi et al[14] have emphasized the decrease in the interfacial energy between matrix and M-A constituent. In fact, several authors observed that the crack propagated preferentially along the interface between the M-A constituent and the matrix, and from this observation they have suggested that the interfacial area between M-A constituent and matrix plays an important role in the crack propagation.

In this investigation, we also observed that the fracture propagated preferentially along the interface between M-A constituent and matrix. Results from the instrumented Charpy-impact test suggested that the massive M-A constituent decreases the crack propagation energy much more significantly than the elongated M-A

constituent. The observation of the microstructure showed that the increase in the total area of M-A constituent with the increase in $\Delta t_{8/5}$ was mainly attributable to the coarsening of the massive M-A constituent (see Fig. 3). It can therefore be concluded that the decrease in fracture propagation energy with the increase in $\Delta t_{8/5}$ is due to the increase in the interfacial area between the massive M-A constituent and the matrix that results from the coarsening of the M-A constituent.

6. Conclusions

The effects of the M-A constituent on the embrittlement of 780 and 980 MPa class HSLA steels undergoing high heat input weld thermal cycles have been investigated metallographically and theoretically. Results obtained are summarized as follows:

(1) The increase in the total area fraction of M-A constituent with the increase in $\Delta t_{8/5}$ was mainly attributable to the coarsening of the massive M-A constituent.

(2) On the ductile fracture surfaces after a slow rate bending test, M-A constituents were observed at the bottom of dimples, suggesting that the M-A constituent acts as a initiation site of dimples.

(3) In the cleavage fracture, M-A constituents were observed at initiation sites of main and secondary cracks. The cleavage fracture propagated preferentially along the interface between M-A constituent and matrix.

(4) Results from the instrumented Charpy-impact test suggest that the massive M-A constituent lowered the crack initiation and propagation energies much more significantly than the elongated M-A constituent.

(5) Results from the FEM analysis indicate that the significant concentration of plastic strain occurs in the soft phase neighboring hard phases of both elongated shape and massive shape. This result corresponds well with the observations that micro-voids were initiated in the neighborhood of the interface between M-A and matrix. The region of the large tensile plastic strain extends over wider area around the massive hard phase than the elongated.

(6) From these results, it can be concluded that the deterioration of absorbed energy with the increase in $\Delta t_{8/5}$ was attributable to the coarsening of the massive M-A constituent.

Acknowledgment

The authors would like to express their sincere thanks to Prof. M. TOYODA, Osaka University for his useful advice on FEM analysis and to Dr. Z.LI (Foreign Researcher, Harbin Institute of Technology) for his cooperation in observing the M-A constituents.

References

1) K.Tanaka, T.Mori, and T.Nakamura: Phil. Mag., **21-2**(1970) 267-279.
2) M.F.Ashby: Phil. Mag., **21-2**(1970) 399-424.
3) T.Tomota, Y.Kawamura, and K.Kuroki: JSME Intern. J., Series A, **46-6**(1980) 598-604 (in Japanese).
4) D.A.Curry and J.F.Knott: Metal Sci., **10-1**(1976) 1-6.
5) B.J.Brindley and T.C.Lindley: JISI, **210-2**(1972) 124-125.
6) C.J.Mcmahon,Jr. and M.Cohen: Acta Metall., **13-6**(1965) 591-604.
7) P.Bowen, S.G.Druce, and J.F.Knott: Acta Metall., **34-6**(1986) 1121-1131.
8) H.Okada, F.Matsuda, and Z.Li: Quarterly J. Japan Weld. Soc., **12-1**(1994) 126-131(in Japanese).
9) H.Okada, K.Ikeuchi, F.Matsuda, I.Hrivnak, and Z.Li: Quarterly J. Japan Weld. Soc., **12-2**(1994) 236-242(in Japanese).
10) H.Okada, F.Matsuda, K.Ikeuchi, and Z.Li: Quarterly J. Japan Weld. Soc., **12- 3**(1994) 398-403(in Japanese).
11) J.H.Chen, Y.Kikuta, T.Araki, M.Yoneda, and Y.Matsuda: Acta Metall., **32-10**(1984), 1779-1788.
12) T.Haze and S.Aihara: Proc. The 7th International Offshore Mechanics and Arctic Engineering Symposium, (1988) 515-523.
13) M.Yoneda: Doctoral Thesis, Osaka Univ. (1985), (in Japanese).
14) M.Nakanishi, Y.Komizo, and Y.Fukada: Quarterly J. Japan Weld. Soc., **4-2**(1986) 447-452(in Japanese).
15) Society of Automotive Engineers : SAE J 417.
16) G.R.Speich, A.J.Schwoeble, and W.C. Leslie : Metall.Trans., **3-8**(1972) 2031-2037.
17) T.Yasuno, K.Kuribayashi, R.Horiuchi, and M.Otsuka: Tetu-to-Hagane, **77-10**(1991) 1725-1732(in Japanese).
18) Y.Ohkomori, I.Kitagawa, K.Shinozuka, T.Toriyama, K.Matsuda, and Y.Murakami: Tetu-to-Hagane, **77-3**(1991) 438-445(in Japanese).
19) K.Satoh, M.Toyoda, T.Terasaki, and S.Kaihara: Journal of The JWS, **46-8**(1977) 572-577(in Japanese).
20) K.Satoh, T.Terasaki, and T.Tanaka: J. Japan Weld. Soc., **48-8**(1979) 616-620(in Japanese).
21) B.C.Kim, S.Lee, N.J.Kim, and D.Y.Lee : Metall.Trans., **22A-1**(1991) 139-149.
22) Hydraulic and Penstock Association : Technical Standards for Gates and Penstocks, 1993.3(in Japanese).
23) Honsyu-Shikoku Bridge Authority : Technical Standard for manufacture of Steel Bridge(in Japanese).
24) Y.Ohmori, H.Ohtani, and T.Kunitake: Tetu-to-Hagane, **57-10**(1971), 1690-1705(in Japanese).
25) Y.Komizo and Y.Fukada: Quarterly J. Japan Weld. Soc., **6-1**(1988) 41-46(in Japanese).
26) F.Kawabata, K.Amano, N.Itakura, F.Minami, M.Toyoda, and H.Jing: Proc. The Workshop on Strength Mismatching and Its Control, (1992) 1-11.
27) F.Minami, H.Jing, M.Toyoda, F.Kawabata, and K.Amano, Proc.The Workshop on Strength Mismatching and Its Control, (1992) 23-34.
28) H.Ohtani, F.Terasaki, and T.Kunitake: Tetu-to-Hagane, **58-3**(1972), 434- 451(in Japanese).